The luminosity achievable in a linac-CESR collider based on the present performances and perspective

P. Patteri - LNF-INFN

September 26, 1997

1 Introduction

Previous estimate of the luminosity achievable on a linac-CESR collider [1] were based on the performance data taken from the literature, which mainly reported results concerning the optimization of operation for the CLEO detector in the South Interaction Point (SIP). Moreover, the linac parameters were taken from the design performances of the TESLA Test Facility superconducting linac and no attempt was done to estimate the luminosity, which could be provided by the existing S-band linac of the CESR injection chain.

The set of the parameters used in this note is derived from past measurements with different configurations or limited extrapolations. Anyway its feasibility must be checked with a machine test; this estimate is intended to define the linac and lattice upgrading required to reach a luminosity of $1 \cdot 10^{30}\, cm^{-2} s^{-1}$ in an experiment at the North Intraction Point (NIP).

The luminosity is given by

$$\mathcal{L} = \frac{n_e n_p f_c}{4\pi\sigma_x\sigma_z} = \frac{I_M I_{CESR}}{4\pi\sigma_x\sigma_z}\frac{t_M f_M}{e^2 n_b f_{ring}}$$

The meaning of the parameters is given in the footnote [1]. In the following chapters their present and achievable values are discussed.

[1] $n_{e(p)}$ is the number of electrons (positrons) in each bunch; f_c $[Hz]$ is the frequency of collision at the interaction point;I_{CESR} $[A]$ is the stored current in CESR, divided in n_b bunches, circulating with orbital frequency f_{ring} $[Hz]$;.I_M $[A]$, t_M $[s]$ and f_M $[Hz]$ are respectively current, duration and repetition rate of the linac macropulse.σ_x, σ_z $[cm]$ are respectively the horizontal and vertical size of the beam at the interaction point.

2 The CESR parameters

A schematic layout of the experiment is shown in fig. 1. The shaded background indicates which new parts, or substantial changes, are required for the linac-ring collider operation. Some of these (lighter background) would improve the injector operation for the standard CERS two beam operation too.

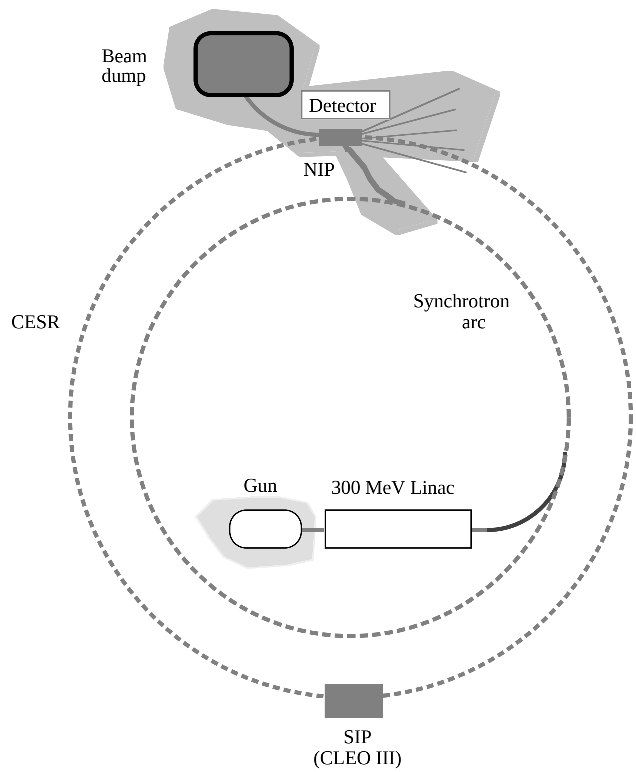

Fig. 1 - Schematic layout of the linac-ring collider at CESR.

2.1 The current

At constant currents I_M and I_{CESR} the luminosity increases as $L \propto n_b^{-1}$, as shown in (1). The reduction of the number of the stored bunches, and the variation of their spacing, affect the multibunch instability threshold. Moreover it implies a corresponding increase of the bunch charge in the electron beam, which usually impairs the emittance, so a trade off must be found.

The best performances achieved at CESR are summarized in table 1. The measurements in column 3 and higher [2], intended to measure the instability threshold in multibunch mode and its dependance on bunch spacing, were carried on without feedback; an improvement of $\approx 50\%$ is usually achieved with the feedback on. The measurements in column 1 and 2 were carried on recently [3]. The feedback was on in the 9 bunch run.It was possible to store without difficulty $52\,mA$ in a single bunch with the feedback off and $200\,mA$ in 9 bunches with the feedback on. In both cases the test was terminated by a trip of the rf system before any instability onset were observable.

The current should be raised in future up to $500\,mA$ with the installation of superconducting cavities. The results in the first two columns of table 1 indicates that this improvement can be fully exploited concentrating the current in a few bunches. Moreover, the sc cavities will reduce the wall impedance raising the instability threshold. If the collider will have dedicated shifts for enough long time, the vertical separators in the North area could also be removed, further improving the wall impedance. This eventually could result as a necessity to realize a suitable interaction region.

All this indicates that $n_p = 5 \cdot 10^{11} \times 18$ bunches or even $n_p \approx 9 \cdot 10^{11} \times 9$ bunches should be possible after the planned upgrading. This possibility is discussed in the following, but it is presumable it could not be fully exploited due to the linac bunch current limit. Anyway this gives the possibility of the choice among different $n_p, n_e,$ and f_c combinations. The number of bunches ≈ 15 fits best with the linac performances reported in the next section.

Table 1: Multibunch instability threshold with different train structures with feedback off (1×9 train with feedback on).

$Bunch \times train$	1×1	1×9	2×9				3×9	4×9
$Spacing\ [ns]$	2560	284	14	28	42	56	6 $pattern$	4 $pattern$
$I_{th}\ [mA]$	52	200	100	183	231	162	155 max	150 max
$n_p/bunch[10^{10}]$	80.0	35.6	8.4	16.3	20.5	14.4	9.2	6.7

Since the collider does not require a close packing of the bunch train to avoid parasitic crossings, a larger bunch spacing can be used to minimize the wakefield effects. The ring can be filled with 15 bunches equally spaced at $168\,ns$, leaving a reduced gap of $42\,ns$ between the first and the last bunch.

The bunch spacing (constrained to multiple integer of $14\,ns$) is relevant to provide negative interference between the wakefield caused by previous bunches. Some measurements [7] clearly show this effect on the wakefield caused by a scraper protruding inside the vacuum chamber when trains of closely spaced bunches are stored. Of course the resonant frequency and the decay time will depend on the discontinuity trapping the wakefield. In our collider the multibunch instability driven by these fields could be tamed by a systematic search of long decay wakefield and fine adjustment of bunch spacing to provide as far as possible a cancellation among them.

2.2 The lattice

The lattice for the present CLEO operation with flat beams has the parameters listed in the first row of the table 2. The operation with round beam is under study; the design parameters are listed in the second row. It will provide a luminosity increase of a factor 1.9. In the following two rows the same parameters at the interaction point are scaled by the emittance reduction factor which should be given by an orbit distortion so that $J_x \approx 2$, as discussed below. The data in the row 4 are just an extrapolation of those in rows 2 and 3 [5].

Table 2: CESR parameters with different lattice at $5.3\,GeV$.

$Configuration$ $type$	β_x $[m]$	β_z $[m]$	ϵ_x $[m \cdot rad]$	ϵ_z $[m \cdot rad]$
$Standard$	1.0	0.015	$1.9 \cdot 10^{-7}$	$5.9 \cdot 10^{-9}$
$Round\ beam$	0.030	0.030	$9.5 \cdot 10^{-8}$	$9.5 \cdot 10^{-8}$
$Standard\,\&\,J_x = 2$	1.0	0.015	$7.2 \cdot 10^{-8}$	$2.2 \cdot 10^{-9}$
$Round\ beam\,\&\,J_x = 2$	0.030	0.030	$3.6 \cdot 10^{-8}$	$3.6 \cdot 10^{-8}$

These optical functions at SIP have been obtained with the permanent magnet quadrupoles of the microbeta insertion; the round beam focusing will require superconducting quadrupoles too. A similar focusing will be provided for the interaction point in the North Hall, moreover, since a collision point displaced a few meters away from the symmetry point is foreseen, a peculiar arrangement of the lattice is required. In the present luminosity estimate it is assumed that the listed values have been achieved in this new arrangement too.

2.3 Effect of change in J_x

The first studies of CESR performances with round beams were carried out in 1990 [9], using a lattice designed to provide only one collision in the NIP.

The separation required in the SIP, displacing in different way the e^- and e^+ trajectories in the strong quadrupoles of the microbeta section, caused a reduction of the positron beam emittance, mainly due to the increase of the partition number J_x up to $J_x = 1.9$. The maximum expected emittance reduction factor was 2.1, as shown in table 3. The beam separation was really set with electrostatic separators [4] and a few measurements of the beam sizes were carried out, confirming that the effect is opposite for e^+ and e^-, although the systematic errors prevented a close comparison with the simulation results[9].

Table 3: CESR parameters (e^+ and e^- beam) vs. separator kick .

$Sep.kick$	$[mrad]$	0.0	± 0.16	± 0.30	± 0.70
D^+		0.02	-0.19	-0.37	-0.91
D^-		0.02	0.23	0.40	0.90
ϵ^+	m	$1.36 \cdot 10^{-7}$	$1.09 \cdot 10^{-7}$	$0.93 \cdot 10^{-7}$	$0.64 \cdot 10^{-7}$
ϵ^-	m	$1.36 \cdot 10^{-7}$	$1.77 \cdot 10^{-7}$	$2.34 \cdot 10^{-7}$	$15.44 \cdot 10^{-7}$
τ_x^+	ms	28.6	23.6	20.4	14.6
τ_x^-	ms	28.6	36.4	47.1	288.6
τ_s^+	ms	13.9	15.5	17.2	25.8
τ_s^-	ms	13.9	12.6	11.7	9.7
$(\sigma_E/E)^+$		$0.60 \cdot 10^{-3}$	$0.63 \cdot 10^{-3}$	$0.67 \cdot 10^{-3}$	$0.81 \cdot 10^{-3}$
$(\sigma_E/E)^-$		$0.60 \cdot 10^{-3}$	$0.57 \cdot 10^{-3}$	$0.55 \cdot 10^{-3}$	$0.50 \cdot 10^{-3}$

Since the source of this effect is limited to the ring arc around the SIP, it could be exploited whatever lattice change is done at NIP.

The increase of the energy spread raises the single bunch current limit too, which could be of concern to exploit the planned current increase to $500\,mA$.

2.4 The ultimate emittance

Another way to reduce the beam size is to use a low emittance lattice, with higher tunes. CESR operated in this configuration for a few runs dedicated to synchrotron radiation user [11], achieving an emittance $\epsilon_x = 5.5 \cdot 10^{-8} @ 5\,GeV$. Since the Touschek effect on lifetime began to be evident [2], this can be considered the ultimate usable emittance. This scales to $\epsilon_x = 6.2 \cdot 10^{-8}$ at $5.3\,GeV$ where of course the Touschek lifetime is slightly longer.

[2] M. Billing, private communication

For comparison the minimum horizontal emittance achievable with a FODO machine with a magnetic layout composed of 80 bends, like CESR, is $\epsilon_x = 5.1 \cdot 10^{-8}\,m$. This could be reduced to $\epsilon_x = 2.4 \cdot 10^{-8}\,m$ with the orbit distortion so that $J_x \approx 2$. Finally, if round beam and full coupling operation is considered, the horizontal and vertical emittance might be $\epsilon_x = 1.2{\cdot}10^{-8}\,m$.

It is to bear in mind that in table 1 a radial-vertical coupling $k = 0.03$ was assumed, as reported in the literature for colliding beam operation. In the linac-ring collider operation, with much smaller beam beam perturbation, the bunch dynamics is essentially that of a single beam, allowing a smaller k. A value $k = 0.01$ is still conservative at current up to $50\,mA/bunch$. In section 5 a comparison of the luminosity achievable with different lattice is carried on, and this factor, providing a luminosity improvement of $\sqrt{3}$, is taken into account.

3 The linac

The linac-ring collider operation needs an electron beam of energy between $150\,MeV$ at the baryon pair threshold and $200\,MeV$ above the Ξ pair threshold. As shown clearly by eq. (1), the luminosity is proportional to the average current $< I >= I_M f_M T_M$. The S-band linac in the injection chain of CESR provides a $337\,MeV$ electron beam. The linac specifications have been closely matched to the synchrotron performances, so probably no power plant oversizing could be exploited to improve the present capability. The limits are mainly set by the HV supply, modulators and maybe klystron. Some improvement is considered feasible, by an overall factor 2, but cannot be guaranteed; moreover, the reliability of a linac continuously operating at its limit must be seriously taken into account. The accelerating guides should be capable of sustaining an higher duty cycle, taking into account the reduced gradient too. The bunch train formation in the $2.56\,\mu s$ macropulse is obtained with a $150\,kV$ grid gun and a prebuncher. This allows a large freedom in the choice of the bunch spacing, but cannot provide a high quality beam at high bunch charge. The most powerful operating mode provides a train of 15 microbunch of 10nC at a repetition rate of $60\,Hz$. The corresponding parameters involved in (1) are $n_e = 6.3 \cdot 10^{10}$ and $f_c = 900\,Hz$.

An emittance measurement [12] gave a normalized transverse emittance $\epsilon^{(n)} = \epsilon\gamma\beta = 1.3 \cdot 10^{-3}$. This corresponds to $\epsilon = 4 \cdot 10^{-6}$@150 MeV and it is two orders of magnitude worse than the emittance required to match the stored beam.

3.1 The linac stability and possible improvements

A number of items to be addressed to improve the injection chain in CESR has been listed in June 1994 [14]. A part of them would be relevant to the operation of the linac for this collider. A program to improve diagnostic and control system of the existing linac would be useful to its operation for CESR and to a better definition of the upgrading which should be included in a proposal for the linac-ring collider.

Since the linac normalized emittance is equal, at the best, at the injector emittance, a new injector providing $\epsilon^{(n)} \approx 4 \cdot 10^{-6} @ 10\, nC$ is required. Such performances are the top (maybe ahead) of the present achievements for the linear collider and FEL injectors. A substantial expertise will be gained in short terms by the study carried on at DESY and Fermilab for the TESLA injector [13]. Such an injector will be based on an rf gun with a photocathode providing a few MeV bunched beam, ready for injection in the first linac section. Due to the better performances in the critical low energy stage it would provide a large improvement in the electron injection efficiency in the synchrotron and in the beam focusing at the positron converter.

Some measurements have been carried out in the past in the high charge mode, resembling the operating mode required for the collider. The existing data are reported here as a reference [6], since most will be positively affected by the lower emittance and higher energy of the new injector. Some other measurements are proposed.

The single bunch emittance degradation in the transport through the accelerating guide must be estimated by simulation; of course no meaningful measurement can be done with the present injector.

The beam position wandering and drift, causing an apparent increase of averaged emittance, could be measured by the existing beam position monitors but care must be taken not to overestimate this effect, which depends on the drift due to the present injector too. Indeed, a drift in the millimeter range due to the wakefield of close bunches has been observed [10]; a larger effect should be expected at $10\, nC/bunch$. Since all this happens to the beam at $\approx 400\, keV$, the new injector will completely overcome these problems.

Two largely different time constants are involved in the linac beam dynamics: the prebuncher filling time $\tau_{PB} \approx 30\, \mu s$ and the accelerating section filling time $\tau_L \approx 700\, ns$.

The beam loading of the 214 MHz prebuncher, resulting mainly in a large phase shift, is compensated by adjustment of the gun timing. The residual phase shifting along the macropulse can be compensated, independently of its cause, by acceleration at $+\Delta\phi$ and $-\Delta\phi$ with respect to the peak in consecutive linac sections, so that the opposite slopes of the accelerating field cancel the effect of the phase jitters. This is done now only in the last two sections.

The energy variation due to beam loading during the macrobunch has been measured with the existing set up. The effect of the beam loading at $\approx 300 MeV$ is $\Delta E/E = 3\%@2 \cdot 10^{10}\ e^-$. This value is taken with respect to the energy of the first bunch in the macropulse and it is due to the integrated charge during the following τ_L. In our case $n_e = 6 \cdot 10^{10}$ so $\Delta E/E = 9\%$ must be assumed; the energy difference among the following bunches at time $> \tau_L$ is lower by an order of magnitude due to balancing between beam loading and rf power feeding at lower accelerating field. Moreover, since operation at 2/3 of the maximum gradient is foreseen, a wide dynamic range is available to farther reduce this energy drift with a feedforward correction.

The energy spread in the microbunch has never been measured directly.

If a current of $500\, mA$ in 10 bunches can be stored in CESR a corresponding linac bunch pattern is desirable. This would imply $15\, nC/bunch = 9 \cdot 10^{10}\, e^-$; the beam loading and the wake field will heavily affect the beam quality. It is not possible to assert now that it is possible to provide such a high charge beam with emittance suitable for the collider.

4 The interaction region

A lattice for the interaction region (IR) has been designed and matched to the low emittance optics used in dedicated synchrotron radiation operation [11]. No attempt to distort the orbit in order to get $J_x \approx 2$ was done.

This design was mainly intended to give an insight to the constraint posed to the detector by the magnetic elements of the lattice, which has to provide a smaller beam section with respect to the lattice already considered [3]. The IR lattice was not constrained to be compatible with standard lattices for two beam operation, but the compatibility seems to be retrievable with further adjustments. The goal of the design were:

- Easy matching to the linac beam.
- Reduced, as far as possible, interference between linac and ring lattice.
- Minimal interference between ring lattice elements and collimated charged pairs.
- Large room for multihadron detection soon after the collision point.
- Asymmetric position with respect to the experimental hall to increase the time of flight usable for particle identification.

It is to note that the angular opening of the pairs is depending on the available kinetic energy in the c.m. frame, weakening any optimization of the third item in the list. Since this is a crucial point to the success of the

[3]The IR design was carried on after a preliminary version of this note showed that the luminosity achievable in standard CESR configuration (current, IR, bunch pattern) had to be improved by nearly an order of magnitude to provide the collider requirements.

experiment, an iterative study of the interference between the detector and the quadrupoles, even realized with different technology, is to be carried on. A much wider presentation of the interaction region and its entanglement with the detector will be given in a separate note.

4.1 The linac and ring beam size matching

The linac emittances are typically equal in both planes, therefore the beam size ratio is

$$\frac{\sigma_z}{\sigma_x} = \frac{\sqrt{\beta_z \epsilon_z}}{\sqrt{\beta_x \epsilon_x}} \approx \frac{\sqrt{\beta_z}}{\sqrt{\beta_x}}$$

A ring with minimal coupling has $\epsilon_z/\epsilon_x \approx 10^{-2}$; moreover, in a microbeta collision point it is $\beta_z/\beta_x < 0.1$ so the beam size ratio is

$$\frac{\sigma_z}{\sigma_x} = \frac{\sqrt{\beta_z \epsilon_z}}{\sqrt{\beta_x \epsilon_x}} < 0.03$$

In order to match such a beam the linac lattice at the interaction point should provide $\beta_z/\beta_x \approx 10^{-3}$.

Clearly, the round beam lattice with $\epsilon_z = \epsilon_x$ best suits to collider operation, but it needs stronger focusing in both planes to obtain the same beam section; superconducting quadrupoles are also required. With such a choice it seems hard to reach the other goals, namely the smallest angular covering of the downstream line.

In an (out-of-coupling) ring lattice a round beam can be obtained with $\beta_z >> \beta_x$; this cannot be done in standard ring because the linear tune shift becomes intolerable, but in the collider the repetition rate $f_M \approx 1/\tau_{damping}$ so the cumulative effect is weighted with a very low duty cycle. The perturbation to the stored beam were a major concern in the design of high luminosity linac-ring collider for the B-factory, mainly due to the dipolar kicks caused by the linac beam wandering. A carefull study of these effects is mandatory after the choice of a lattice with $\beta_z >> \beta_x$, which appears the more feasible at this stage.

The beam section Σ is given by

$$\Sigma = \sigma_x \sigma_z = \begin{cases} \epsilon_x \beta_x / 2 & \textit{for round beams} \\ \epsilon_x \sqrt{k \beta_x \beta_z} & \textit{for flat beams} \end{cases}$$

With the round beam parameters $\beta_x = \beta_z = 0.03\,m$ and $\epsilon_x = \epsilon_z = \frac{1}{2} 6.2 \cdot 10^{-8}$ it is $\Sigma = 9 \cdot 10^{-10}$. In order to obtain the same Σ with the flat beam and $k = 0.01$ it must be $\beta_x \beta_z = 0.0225\,m^2$.

4.2 The lattice of the IR

The lattice has $\beta_x = 0.022\,m, b_z = 0.293\,m \rightarrow \beta_x\beta_z = 0.0064\,m^2$, providing a luminosity improvement of a factor ≈ 1.9 with respect to previous assumption. A dispersion free straight section ($\eta \approx 0$) is mandatory so that $\eta \cdot (\sigma_E/E) < \beta_x\epsilon_x$ and the contribution to the radial beam size due to the energy spread is negligible. At CESR it is $\sigma_E/E = 6 \cdot 10^{-4} @ 5.3\,GeV$ so must be $\eta < 0.06\,m$. This is fulfilled adjusting the four quadrupoles upstream the last magnet, although not a perfect dispersion suppression has been achieved leaving a residual $\eta = 0.02\,m$ at the IP. The terminal part of the West arc modified to realize the dispersion suppressor is shown in fig. 2.

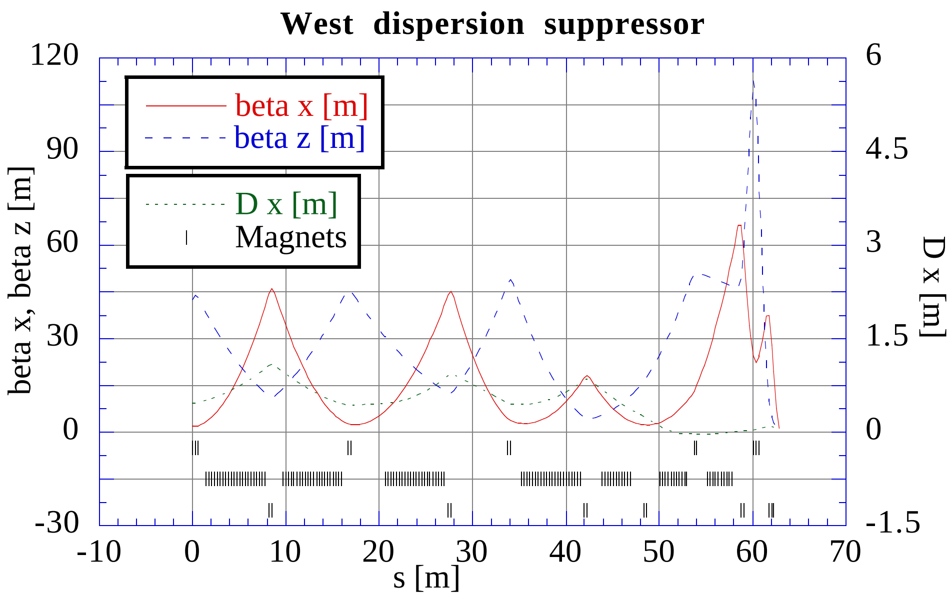

Fig. 2 - Optical functions β_x, β_z, η_x in the West arc modified for dispersion suppression. The magnetic elements are displayed with thick points.

The requirement of an asymmetric position suggested to realize a waist as soon as possible after the last upstream magnet, using most of the straight section for matching at the first downstream magnet, so as not to affect the dispersion suppressor. Eventally a completely symmetric layout came out, with two waists $7\,m$ apart. This may not to be the best solution, since special quadrupoles are used around the waists and limited free space is available between the central quadrupoles. However, this provides $1.5\,m$ free downstream the interaction point and $0.8\,m$ upstream; a collision angle less than 0.1 radian is feasible guiding the electron beam with a septum magnet up to a few centimeters from the axis.

The optical functions of the lattice in the IR region are shown in fig.3. The description of the elements layout and strength, and the optical functions produced by MAD are given in appendix. A more detailed discussion of the magnet occupancy is given in the following.

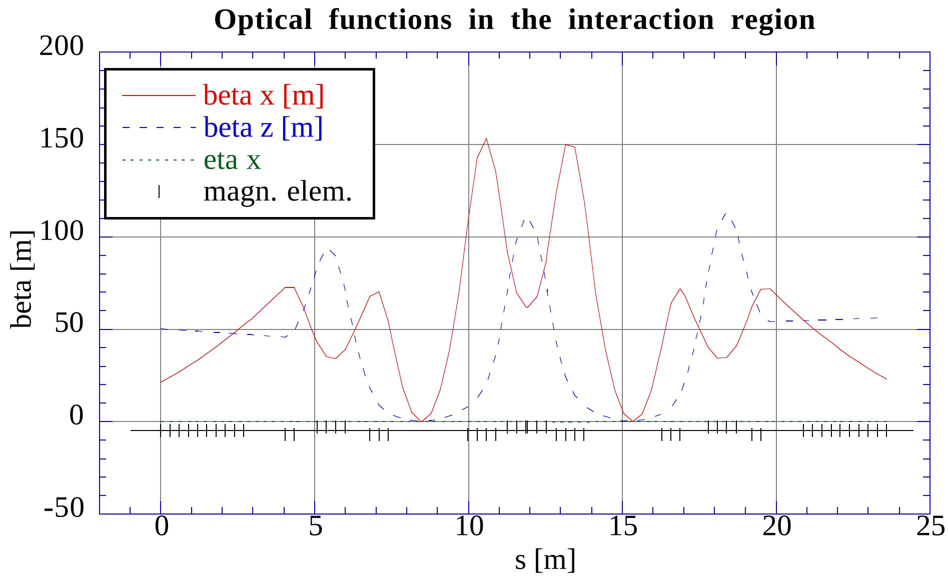

Fig. 3 - Optical functions β_x, β_z in the interaction region.

It is to note that the free space after the last magnet, which is $\approx 3.4\,m$ in the standard CESR lattice, is now reduced to $1\,m$. It is partially occupied by the vertical separators, so there is no compatibility between the standard and collider lattices; however, a shorter version of the IR lattice, with less room after the IP, could be matched proviging more room for the separators. Anyway it is wortwhile noting that the higher β_z in collider lattice increases the effectiveness of a vertical kick compensating for a shorter separator.

4.3 The magnet occupancy

The magnets downstream the IP have strength [4] $K1 \geq 1\,m^{-2}$. If realized with the conventional electromagnet tecnology they would occupy a large space around the pipe. The permanent magnet (PM) quadrupoles provide $K1 > 1.5\,m^{-2}$ and have a far smaller outer radius. The parameters of the PM quadrupoles for the CESR phase III IR have been taken as a reference and are listed in table 4, together with those for the collider IR. Their transverse mechanical dimension have been assumed to define the allowed geometrical acceptance of the detector, although the collider quadrupoles, due to the lower $K1$, could probably be slightly smaller. The space Δz is measured from the IP and the nearest edge of the element. The masked angles are measured with respect to the positron beam axis.

[4] The MAD notation is used here: $K1 = \frac{\partial B}{\partial x} \cdot \frac{1}{B\rho}$

Table 4: Parameters of the PM magnets

Machine config.	*Magnet type*	$K1$ $[m^{-2}]$	Δz $[m]$	*length* $[m]$	*i.rad.* $[cm]$	*o.rad.* $[cm]$	*Masked angle*
CESR III	*REQ1*	-1.63		0.094	3.35	6.40	
"	*REQ2*	-1.78		0.188	3.35	7.04	
Collider	*QWN1*	1.56	-0.80	0.760	3.35	6.4	$\theta < 0.043$
"	*QWN2*	-0.94	-2.45	0.950	3.35	6.4	
"	*QEN1*	1.06	1.80	0.990	3.35	6.4	$\pi - 0.069 < \theta$
"	*QEN2*	-1.00	2.78	0.650	3.35	6.4	
"	*Bend*	$--$	12.40	2.945	2.50	$--$	$0.0016 < \theta$

The trajectories of all particles exiting at angle $0.043 < \theta < \pi - 0.069$ with respect to the positron direction are free of any interference from the magnetic elements.

The total solid angle free from interference is $> 0.99 \times 4\pi$. However, the angular acceptance must be weighted by the angular distribution in the laboratory frame, which is strongly depending on the particle kinetic energy in the center of mass frame. The geometrical cuts caused by the quadrupoles are shown in fig. 4.

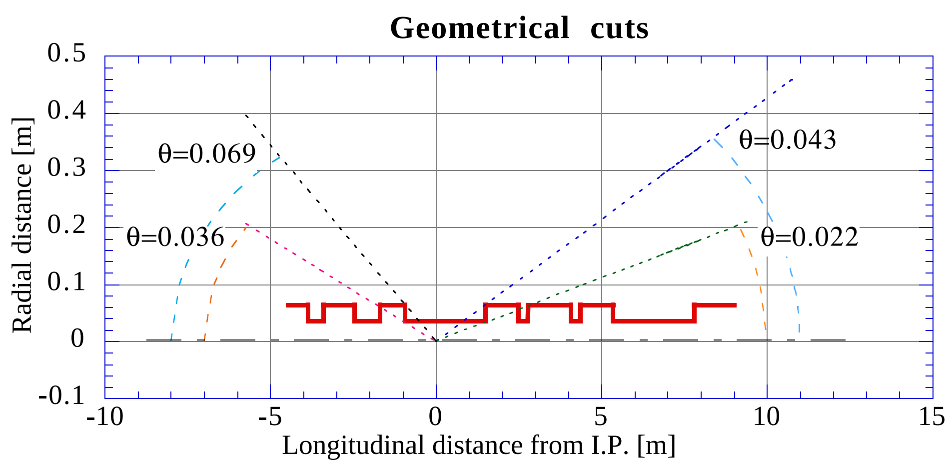

Fig. 4 - Geometrical cuts due to the outer radii (thicker line) of the quadrupoles around the interaction region.

The particles at angle $0.022 < \theta < 0.043$ and $\pi - 0.069 < \theta < \pi - 0.036$ exit the vacuum pipe at distance from the interaction point $\Delta z < 1.50\,m$ and $\Delta z < 0.93\,m$ and go through the body of the first downstream and upstream quadrupole respectively. Due to the thinness of the PM quadrupoles $\approx 3\,cm$ a non negligible detection efficiency for these particles is conceivable. On the other hand, this could be the source of a strong background generated by the conversion of γ's coming from the upstream bending magnet.

From the upstream waist to the end of the first downstream bend there are $15.4\,m$ and a full opening angle of 3.2 milliradian in the vertical plane and someting more in the radial plane, depending on the pipe width inside the magnet. It could be useful for measurements of barions just a few MeV above the threshold.

5 The luminosity

The starting point of this feasibility study were the parameters listed in [8], coupled with the achievements of the linac and ring currents reported in sect. 2 and 3. This corresponds to the first line of the table 5.

Table 5: Luminosity achievable as a function of various CESR configuration.

$Config.$	ϵ_x $[nm]$	k	$4\pi\Sigma \cdot 10^8$ $[cm^{-2}]$	n_p $[10^{11}]$	n_e $[10^{10}]$	f_c Hz	$\mathcal{L} \cdot 10^{30}$ $[cm^{-2}s^{-1}]$
$Standard\,(flat\ beam)$	190	0.03	5.06	3	6	900	0.03
$Standard\,\&\ J_x \approx 2.$	90	0.03	2.39	3	6	900	0.07
$\epsilon_{min}\ (f.b.)$	51	0.03	1.36	3	6	900	0.12
$\epsilon_{min}\ \& J_x \approx 2\ (f.b.)$	24	0.03	0.64	3	6	900	0.25
$\epsilon_{min}\ (r.b.)$	26	1.00	0.96	3	6	900	0.17
$\epsilon_{min}\ \& J_x \approx 2\ (r.b.)$	12	1.00	0.45	3	6	900	0.36
$LatticeSR$	62	0.01	0.62	5	6	900	0.43
$LatticeSR\&J_x \approx 2.$	29	0.01	0.29	5	6	900	0.92
$LatticeSR\&J_x \approx 2.$	29	0.01	0.29	9	6	900	0.99
$LatticeSR\&J_x \approx 2.$	29	0.01	0.29	9	9	540	1.49
$\epsilon_{min}\&J_x \approx 2.$	24	0.01	0.24	9	9	540	1.80

The improvements due to lattices with lower emittance are in rows 2 - 4. The further conceivable improvements using a round beam are in rows 5 and 6. All these configurations use an IR lattice not optimized for collider operation and in the flat beam cases assume $k = 0.03$, as reported in the colliding beam literature.

The following data (rows 7 - 11) refer to the IR lattice briefly described in sect. 4 and take into account the possible increase of n_p and n_e when CESR current $\approx 500\,mA$.

These evaluations has been carried out at $5.3\,GeV$; operation at reduced energy down to $\approx 4.0\,GeV$ can give a factor 1.7, due to the decreased emittance, but all beam stability issues at high current and the compatibility with the permanent magnets in the SIP must be considered.

6 Conclusion

A linac-ring collider based on CESR and the existing injector seems feasible. It can provide the required luminosity $\mathcal{L} = 10^{30} cm^{-2} s^{-1}$ exploiting the planned machine upgrading, a low emittance lattice and a new interaction region.

The linac emittance must be reduced using a new gun which will improve the overall linac stability and positron injection efficiency. Further test on the linac emittance stability along the macropulse are needed.

The possibility of using the existing transfer line from the linac exit to the synchrotron and the synchrotron arc to transport the $150\,MeV$ e^- beam to the North hall is still to be considered. The fundamental question is if such transfer line preserves the beam emittance in a $\approx 200\,m$ long path.

7 Acknowledgment

I am grateful to Prof. K. Berkelman for his kind hospitality at Wilson Laboratory. Warm thanks are due to F. Ceradini, P. Laurelli and P. Campana for allowing my stage. It is a pleasure to thank D. Rice for his interest in this project and the friendly collaboration with which he supported me in any time. I wish to thank all other peoples which were always kindly ready to let me know every information about CESR and the linac I needed, in particular M. Billing. Finally, I wish to thank R. Baldini, who is the entusiastic promoter and supporter of this project, G.C. Moneti, for his help in introducing to the Wilson Laboratory.

References

[1] Proceeding of 1997 LaTuile Workshop

[2] M.Billing and al. , paper presented at PAC 97

[3] Machine study run of 8-12-97

[4] Machine study runs on January-March 1990

[5] The sources of data are: row 1-2 ref. [8], row 3 ref. [9] scaled to take into account the energy difference with respect to the original data at $5.0\,GeV$

[6] M.Billing, private communication

[7] A.Temnykh, 'Wake Field Study Using Two Spaced Bunches', CON 95-06

[8] The CESR/CLEO upgrade project, CLNS 93/1265

[9] P.P.Bagley,Ph.D. Dissertation, Cornell University 1995

[10] C.Y.Tan and L.N.Hand, 'Wake Field Effects of Bunch Trains in the Injector', CON 96-11

[11] Lattices 569E85K785.GE1_5S_U and 539E85K687.GE1_5S_E

[12] V.I.Kazacha and V.H.Prymmer, 'Transverse-emittance measurement in the electron bunches in the linac', CON 94-21

[13] A VUV Free Electron Laser at the TESLA Test Facility at DESY - Conceptual Design Report, TESLA FEL 95-3, DESY 1995;

[14] D. Sagan, 'Note on the Injection Chain into CESR', CON 94-17

Table A1 - MAD input/output files of the interaction region.

```
!Interaction region for linac-ring collider
!
! Drift spaces
dw1:drift,l=0.762
dw3:drift,l=1.08
dw2:drift,l=0.460
de1:drift,l=0.290
de3:drift,l=0.70
de2:drift,l=0.7
dwir:drift,l=0.93
deir:drift,l=1.5
!
dw03:drift,l=0.15714
dw04:drift,l=0.87304
dw07:drift,l=0.50175
dw27:drift,l=2.39981
dw28:drift,l=3.34000
dw45:drift,l=0.85380
dw46:drift,l=1.10564
dw47:drift,l=0.79013
dw50:drift,l=3.64560
dw51:drift,l=0.18260
dw53:drift,l=1.32600
!
! Quadrupoles
!
qwn1:quad,l=0.76,k1=1.5586
qwn2:quad,l=0.95,k1=-0.9424461
qwn3:quad,l=0.6,k1=0.7754535
qen1:quad,l=0.99,k1=1.0587
qen2:quad,l=0.65,k1=-0.9995
qen3:quad,l=0.60,k1=-0.8643
!
! Standard CESR quads
qw45:quad,l=0.60,k1=-0.252217
qw46:quad,l=0.60,k1=0.415909
qw47:quad,l=0.60,k1=-0.196707
qw50:quad,l=0.60,k1=-0.049276
!
! CESR quads modified for matching
qw41:quad,l=0.60,k1=-0.263807
qw42:quad,l=0.60,k1=0.363310
qw43:quad,l=0.60,k1=-0.196539
qw44:quad,l=0.60,k1=0.359481
qw45:quad,l=0.60,k1=-0.2976499
qw46:quad,l=0.60,k1=0.4568916
qw47:quad,l=0.60,k1=0.0522434
qw48:quad,l=0.60,k1=0.551317
qw49:quad,l=0.95,k1=-0.639611
qw50:quad,l=0.60,k1=-0.1618356
!
!
!
!
```

```
!
!
!BENDINGS
b1:sbend,l=6.574262,angle=0.07479974
6,&
  e1=0.018699937,e2=0.018699937
b2:sbend,l=3.237903,angle=0.10228940
1
b3:rbend,l=2.94526,angle=0.020944245
b4:rbend,l=1.6435,angle=0.018699463
b6:rbend,l=3.28698,angle=0.037400331
b7:sbend,l=3.177222,angle=0.09125445
b8:sbend,l=6.575288,angle=0.11220000
7,&
  e1=0.02805,e2=0.02805
!
marc:marker
mip:marker
! LATTICE & LINES
wir:line=(-(b3,dw3,qwn3,dw2,qwn2,&
         dw1,qwn1,dwir,mip))
eir:line=(deir,qen1,de1,qen2,de2,qen3,d
e3,b3)
midir:line=(-wir,deir,qen1,de1,qen2)
fullir:line(midir,-midir)
b:line=(dw03,b1,dw04)
matchw:line=(dw47,qw50,dw07,b7,dw4
6,&
         qw47,dw45,b6,dw53,&

qw46,dw51,b8,dw04,qw45,dw28,&

dw27,qw44,dw51,b8,dw50,qw43,&
         b,qw42,b,qw41)
matche:line=(matchw)
dxzero:line=(-matchw,marc,b3)
arcir:line=(-matchw,marc,-wir)
ir:line=(-wir,eir,matche)
use,fullir
print,fullir[1]
twiss,betx=21.391,bety=50.351,dx=-
0.025,&
    alfx=-4.417,alfy=0.620,dpx=-
0.002,tape
stop
```

Table A1 following

Session Name: CESR10.lns.cornell.edu 2   Page 1

"MAD" Version: 8.9/0   Run: 13/08/97 11.02.15

Linear lattice functions.   TWISS   line: FULLIR   range: #S/#E

Delta(p)/p: 0.000000   symm: F   super: 1   page 1

ELEMENT SEQUENCE				HORIZONTAL								VERTICAL						
pos. no.	element name	occ. no.	dist [m]	betax [m]	alfax [1]	mux [2pi]	x(co) [mm]	px(co) [.001]	Dx [m]	Dpx [1]	betay [m]	alfay [1]	muy [2pi]	y(co) [mm]	py(co) [.001]	Dy [m]	Dpy [1]
begin	FULLIR	1	0.000	21.391	-4.417	0.000	0.000	0.000	-0.025	-0.002	50.351	0.620	0.000	0.000	0.000	0.000	0.000
begin	MIDIR	1	0.000	21.391	-4.417	0.000	0.000	0.000	-0.025	-0.002	50.351	0.620	0.000	0.000	0.000	0.000	0.000
begin	WIR	1	0.000	21.391	-4.417	0.000	0.000	0.000	-0.025	-0.002	50.351	0.620	0.000	0.000	0.000	0.000	0.000
1	B3	1	2.945	55.724	-7.241	0.014	0.000	0.000	0.000	0.019	46.916	0.546	0.010	0.000	0.000	0.000	0.000
2	DW3	1	4.025	72.482	-8.276	0.016	0.000	0.000	0.020	0.019	45.769	0.516	0.013	0.000	0.000	0.000	0.000
3	QWN3	1	4.625	62.560	23.245	0.018	0.000	0.000	0.028	0.007	59.050	-24.673	0.015	0.000	0.000	0.000	0.000
4	DW2	1	5.085	43.005	19.265	0.019	0.000	0.000	0.032	0.007	83.934	-29.423	0.016	0.000	0.000	0.000	0.000
5	QWN2	1	6.035	40.307	-15.661	0.023	0.000	0.000	0.054	0.043	66.763	42.058	0.018	0.000	0.000	0.000	0.000
6	DW1	1	6.797	67.721	-20.316	0.026	0.000	0.000	0.087	0.043	18.059	21.857	0.022	0.000	0.000	0.000	0.000
7	QWN1	1	7.557	40.991	44.240	0.028	0.000	0.000	0.079	-0.063	3.239	3.170	0.040	0.000	0.000	0.000	0.000
8	DWIR	1	8.487	0.022	-0.187	0.303	0.000	0.000	0.020	-0.063	0.293	-0.002	0.242	0.000	0.000	0.000	0.000
9	MIP	1	8.487	0.022	-0.187	0.303	0.000	0.000	0.020	-0.063	0.293	-0.002	0.242	0.000	0.000	0.000	0.000
end	WIR	1	8.487	0.022	-0.187	0.303	0.000	0.000	0.020	-0.063	0.293	-0.002	0.242	0.000	0.000	0.000	0.000
10	DEIR	1	9.987	108.068	-71.844	0.522	0.000	0.000	-0.075	-0.063	7.977	-5.120	0.461	0.000	0.000	0.000	0.000
11	QEN1	1	10.977	124.804	61.235	0.523	0.000	0.000	-0.092	0.032	42.974	-41.688	0.471	0.000	0.000	0.000	0.000
12	DE1	1	11.267	91.815	52.520	0.523	0.000	0.000	-0.082	0.032	70.557	-53.423	0.471	0.000	0.000	0.000	0.000
13	QEN2	1	11.917	61.763	0.046	0.525	0.000	0.000	-0.078	-0.018	111.031	0.176	0.473	0.000	0.000	0.000	0.000
end	MIDIR	1	11.917	61.763	0.046	0.525	0.000	0.000	-0.078	-0.018	111.031	0.176	0.473	0.000	0.000	0.000	0.000
begin	MIDIR	2	11.917	61.763	0.046	0.525	0.000	0.000	-0.078	-0.018	111.031	0.176	0.473	0.000	0.000	0.000	0.000
14	QEN2	2	12.567	91.658	-52.338	0.526	0.000	0.000	-0.107	-0.076	70.217	53.517	0.474	0.000	0.000	0.000	0.000
15	DE1	2	12.857	124.529	-61.009	0.527	0.000	0.000	-0.129	-0.076	42.609	41.684	0.475	0.000	0.000	0.000	0.000
16	QEN1	2	13.847	107.689	71.683	0.528	0.000	0.000	-0.131	0.073	7.560	5.192	0.485	0.000	0.000	0.000	0.000
17	DEIR	2	15.347	0.021	0.095	0.761	0.000	0.000	-0.021	0.073	0.304	-0.355	0.759	0.000	0.000	0.000	0.000
begin	WIR	2	15.347	0.021	0.095	0.761	0.000	0.000	-0.021	0.073	0.304	-0.355	0.759	0.000	0.000	0.000	0.000
18	MIP	2	15.347	0.021	0.095	0.761	0.000	0.000	-0.021	0.073	0.304	-0.355	0.759	0.000	0.000	0.000	0.000
19	DWIR	2	16.277	41.122	-44.290	1.022	0.000	0.000	0.048	0.073	4.162	-3.793	0.914	0.000	0.000	0.000	0.000
20	QWN1	2	17.037	67.784	20.427	1.024	0.000	0.000	0.076	-0.006	21.941	-26.233	0.928	0.000	0.000	0.000	0.000
21	DW1	2	17.799	40.236	15.725	1.026	0.000	0.000	0.071	-0.006	80.157	-50.166	0.931	0.000	0.000	0.000	0.000
22	QWN2	2	18.749	42.723	-19.047	1.030	0.000	0.000	0.098	0.065	100.164	35.446	0.933	0.000	0.000	0.000	0.000
23	DW2	2	19.209	62.048	-22.964	1.032	0.000	0.000	0.128	0.065	70.210	29.671	0.933	0.000	0.000	0.000	0.000
24	QWN3	2	19.809	71.777	8.287	1.033	0.000	0.000	0.147	0.000	54.047	-0.272	0.935	0.000	0.000	0.000	0.000
25	DW3	2	20.889	55.009	7.238	1.036	0.000	0.000	0.147	0.000	54.658	-0.293	0.938	0.000	0.000	0.000	0.000
26	B3	2	23.835	20.793	4.380	1.050	0.000	0.000	0.176	0.020	56.533	-0.343	0.947	0.000	0.000	0.000	0.000
end	WIR	2	23.835	20.793	4.380	1.050	0.000	0.000	0.176	0.020	56.533	-0.343	0.947	0.000	0.000	0.000	0.000
end	MIDIR	2	23.835	20.793	4.380	1.050	0.000	0.000	0.176	0.020	56.533	-0.343	0.947	0.000	0.000	0.000	0.000
end	FULLIR	1	23.835	20.793	4.380	1.050	0.000	0.000	0.176	0.020	56.533	-0.343	0.947	0.000	0.000	0.000	0.000

total length =	23.834520	mux =	1.049846	muy =	0.946689
delta(s) =	0.000000 mm	dmux =	-1.388149	dmuy =	-1.662521
		betax(max) =	124.803520	betay(max) =	111.031177
		Dx(max) =	0.176486	Dy(max) =	0.000000
		Dx(r.m.s.) =	0.089078	Dy(r.m.s.) =	0.000000